

Luminance Thresholds and Their Correlation With Retinal Structure in X-Linked Retinoschisis

J. Jason McAnany,^{1,2} Jason C. Park,¹ Gerald A. Fishman,^{1,3} and Robert A. Hyde¹

¹Department of Ophthalmology and Visual Sciences, University of Illinois at Chicago, Chicago, Illinois, United States

²Department of Bioengineering, University of Illinois at Chicago, Chicago, Illinois, United States

³The Pangere Center for Inherited Retinal Diseases, The Chicago Lighthouse, Chicago, Illinois, United States

Correspondence: J. Jason McAnany, University of Illinois at Chicago, Department of Ophthalmology and Visual Sciences, 1855 W. Taylor St., MC/648, Chicago, IL 60612, USA; jmcana1@uic.edu.

Received: July 19, 2021

Accepted: October 1, 2021

Published: October 27, 2021

Citation: McAnany JJ, Park JC, Fishman GA, Hyde RA. Luminance thresholds and their correlation with retinal structure in X-linked retinoschisis. *Invest Ophthalmol Vis Sci.* 2021;62(13):25. <https://doi.org/10.1167/iovs.62.13.25>

PURPOSE. To provide a comprehensive analysis of light- and dark-adapted luminance thresholds and their associations with retinal structure in X-linked retinoschisis (XLRs).

METHODS. Nine subjects with XLRs and 10 visually-normal individuals participated. Threshold was measured at 15 locations along the horizontal meridian of the visual field at several adaptation levels (5×10^{-5} to 50 cd/m^2) after dark-adaptation. The relationship between threshold and adaptation level across the field was described using a standard “threshold-versus-illuminance” model. Optical coherence tomography images were obtained and segmented to quantify outer nuclear layer (ONL⁺) and outer segment (OS⁺) thickness. A linear structure-function model was used to describe the relationship between threshold and the product of ONL⁺ and OS⁺ thickness.

RESULTS. For peripheral field measurements, thresholds were generally normal for most subjects with XLRs. All subjects had perifoveal and parafoveal threshold elevations under dark-adapted and high illuminance conditions, with thresholds at moderate illuminances being closer to normal. For foveal measurements, seven of nine subjects with XLRs had normal dark-adapted thresholds, and all had abnormally elevated high illuminance thresholds. Threshold-versus-illuminance curves in the fovea, parafovea, and perifovea were abnormally steep for subjects with XLRs, appearing similar to the normal peripheral field shape. Under both dark- and light-adapted conditions, threshold was predicted by ONL⁺ × OS⁺ thickness at nearly all field locations.

CONCLUSIONS. Threshold elevation in XLRs is complex, depending on both the adaptation level and the visual field location. The pattern of threshold-versus-illuminance suggests that macular function in XLRs is similar to the periphery of controls.










Keywords: X-linked retinoschisis, visual field, retinal thickness, visual function, threshold

X-linked retinoschisis (XLRs) is a juvenile onset vitreo-retinal degenerative disease that affects approximately 1:15,000 to 1:30,000 males.¹ XLRs is a monogenic disorder that is caused by mutations in the *Retinoschisin 1 (RS1)* gene²⁻⁴ that is often characterized by cystic-appearing macular lesions. Peripheral retinoschisis, most frequently in the temporal retina, is present in approximately 50% of patients.³ Optical coherence tomography (OCT) imaging has shown that the retina is often abnormally thick because of the schitic cavities, whereas the photoreceptor layer can be abnormally thin, suggesting structural abnormalities of the photoreceptors.⁵ Adaptive optics imaging supports structural abnormalities of the photoreceptors, with cones that appear swollen⁶ and have increased spacing within the area of macular schisis.⁷

In addition to structural abnormalities, functional deficits including a loss of visual acuity (VA) and abnormal electroretinograms (ERGs) are well described in the literature.^{3,8,9} Although VA is not correlated with total retinal thickness⁵ or cystic cavity volume,¹⁰ there is a strong correlation with photoreceptor outer segment thickness.⁵ Other less common measures of visual function have been

reported to be abnormal, including reading speed,¹⁰ shape discrimination hyperacuity,⁵ integration perimetry,⁵ pupillary light reflexes,¹¹ and contrast sensitivity (CS) for grating targets.¹² Visual field perimetry has also been performed in several studies of XLRs, using kinetic,^{7,10,13-15} static,^{7,10,16} and microperimetric^{7,17-19} techniques. The extent of field abnormality varies among these studies, in part because of the variety of techniques used. For example, kinetic perimetry studies^{7,10,13-15} have reported that some, but not all, patients with XLRs have field restriction, with the extent of abnormality depending on target size. Likewise, static perimetry and microperimetry abnormalities have been reported to be variable among patients, with some patients having modest sensitivity loss and others performing normally.^{7,10,16,19} Adaptation level is an important consideration in studies of visual field perimetry. Of the static perimetry reports, two were performed under photopic conditions,^{7,10} four were performed under mesopic conditions,^{7,17-19} and one was performed under scotopic conditions.¹⁶ To date, sensitivity loss has not been compared across different adaptation levels in subjects with XLRs. Such a comparison could provide insight into the relative loss of

TABLE. Subject Characteristics

Subject No.	Color Code	Age (yrs)	Acuity (log MAR)	RS1 Variant	CAI Treatment
1		18	0.52	c.214G>A (p.Glu72Lys)	Diamox
2		19	0.68	c.218C>A (p.Ser73*)	No
3		21	0.58	Deletion of exons 1 – 5	No
4		25	0.36	Deletion of exon 2	No
5		34	0.56	c.578C>T (p.Pro193Leu)	No
6		35	0.60	c.422G>A (p.Arg141His)	Diamox
7		37	0.66	c.208G>A (p.Gly70Ser)	No
8		40	0.40	c.208G>A (p.Gly70Ser)	No
9		49	0.60	c.286T>C (p.Trp96Arg)	No

sensitivity within the rod- and cone-pathways in these individuals.

Thus, the purpose of the present study was to measure and compare psychophysical thresholds across a broad range of adaptation levels in individuals who have confirmed *RS1* mutations to provide a comprehensive analysis of light- and dark-adapted threshold and the associations with retinal structure. Measurements were performed across the visual field to determine how light- and dark-adapted luminance threshold varies as a function of retinal eccentricity in XLRS, as compared to visually-normal individuals. Finally, macular luminance thresholds under dark- and light-adapted conditions were correlated with retinal thickness to better define the relationship between visual sensitivity loss and retinal structure in XLRS.

METHODS

Subjects

The project was approved by an institutional review board of the University of Illinois at Chicago and tenets of the Declaration of Helsinki were followed. All subjects provided written informed consent prior to participating. Nine unrelated male subjects with a clinical diagnosis of XLRS (ages 18 to 49 years; mean of 31 years) were recruited from the cohorts of the Chicago Lighthouse and the University of Illinois at Chicago. The clinical diagnosis of XLRS was based on characteristic fundus features including a spoke-wheel pattern of macular schisis, cystic-appearing macular lesions on OCT, and functional abnormalities including VA loss and a reduced ERG b/a amplitude ratio. A mutation in the *RS1* gene was documented in each individual. The Table lists the age, visual acuity, *RS1* mutation, and carbonic anhydrase inhibitor use at the time of testing. Of note, subjects 3 and 4 had mutations encompassing exons 1–3, which may cause a more severe phenotype than mutations encompassing exons 4–6.²⁰ Ten visually-normal control subjects (six male and four female; ages 23 to 42 years; mean of 29 years) with no history of eye disease, ETDRS best-corrected VA of 0 log MAR or better, and normal contrast sensitivity assessed with the Pelli-Robson chart also participated in the study.

Apparatus, Stimuli, and Procedure

All stimuli were generated by and presented in a commercially available Octopus 900 Pro perimeter (Haag-Streit, Bern, Switzerland). Test targets consisted of blue (449 nm peak) spots of light that were 0.43° (Goldmann III) and were presented for 100 ms. These test targets were presented at

15 locations along the horizontal meridian of the visual field, from 45° temporal to 60° nasal. Thresholds were measured with a 4-2-1 staircase protocol. The targets were presented either in the dark (no background) or against an achromatic field that ranged from 5×10^{-5} to 50 cd/m² in seven steps that were each separated by approximately 1 log unit. Neutral density filters were inserted in the path of the background light source to achieve the four lowest background luminance levels.

Before testing, subjects were dark-adapted for 30 minutes. Appropriate refractive correction was used for test targets presented within the central 20° and removed for targets presented more peripherally. All testing was performed monocularly, with the fellow eye patched. Measurements were obtained from the right eye of each control subject. For the subjects with XLRS, the eye with the best visual acuity was tested (the right eye was tested for eyes of equal acuity). Data obtained from the left eye were replotted in right eye format to facilitate comparisons. Pupil size was recorded by the instrument for each background level and pupil area was used to convert background and stimulus luminance to Trolands.

Threshold data obtained at the different background illuminance levels were modeled using a standard equation^{21–23}:

$$\log T = \log T_0 + \log((A + A_0)/A_0)^n, \quad (1)$$

where T is threshold, T_0 is the absolute dark-adapted threshold, A is background intensity, A_0 is a constant “dark-light” value, and n is a gain (slope) constant.

Optical coherence tomography (OCT) was performed with an Optos OCT/SLO/microperimeter (Optos, Inc., Marlborough, MA, USA) that we have described elsewhere.^{24–26} One high-resolution SD-OCT b-scan, composed of an average of approximately 30 individual scans, was obtained along the horizontal meridian through the fovea. The OCT was segmented using a semiautomated approach^{24,25,27} that was performed in MATLAB using custom-written software. The thicknesses of three layers were quantified: (1) the “total retinal thickness,” defined as the distance between the border of the vitreous/nerve fiber layer and the border of Bruch’s membrane/choroid (BM/Ch); (2) the outer nuclear layer + outer plexiform layer (“ONL⁺”), defined as the distance between the border of the inner nuclear layer/outer plexiform layer (INL/OPL border) and the inner segment ellipsoid (ISE); (3) outer segments + RPE (“OS⁺”), defined as the distance between the ISE and the BM/Ch.

Outer retinal thickness measurements were compared to light- and dark-adapted thresholds, because outer-retina thickness was not confounded by schitic cavities in our sample of subjects with XLRS. The approach to structure-function modeling was based on that described by Jacobson et al.^{28,29} for ONL⁺ structure-function measures and expanded upon by Rangaswamy et al.³⁰ to include ONL⁺ × OS⁺ structure-function measures. In brief, the product of normalized ONL⁺ × OS⁺ was used as the measure of retinal structure for comparison to sensitivity. The normalized ONL⁺ × OS⁺ was computed by dividing each subject’s ONL⁺ × OS⁺ for a given retinal location by the mean control ONL⁺ × OS⁺ measured at the same location. This value is plotted as a function of sensitivity loss, which was also normalized to the control mean measured at the corresponding field location. In this model, it is assumed that the number of photoreceptors is proportional to ONL⁺ thickness and the OS length is proportional to OS⁺ thickness (both measured

by OCT).^{28–30} Consequently, the product of these measurements should be a better measure of quantum absorption than either measure alone.³⁰ Indeed, in individuals who have retinitis pigmentosa, the product of ONL thickness and OS thickness was shown to have a stronger linear relationship with visual field sensitivity than either measure alone.³⁰ Furthermore, if there is thinning of both the ONL⁺ and OS⁺, the product of these measures permits capturing thinning within both layers.

RESULTS

Figure 1 plots log threshold along the horizontal meridian for each subject with XLRS under light- and dark-adapted conditions. Under dark-adapted conditions, it is presumed that threshold is mediated by the rod pathway, with the

exception of measurements performed in the rod-free fovea. Conversely, under light-adapted conditions, it is presumed that threshold is mediated by the cone pathway at all retinal locations. Overall, thresholds were measurable across the visual field for the subjects with XLRS, with few exceptions, including within the central macula, the area of most apparent schitic cavities. Scotomas were observed peripherally in some subjects with XLRS (omitted data points). The pattern of data obtained for the subjects with XLRS under light- and dark-adapted conditions was similar to that of the controls. That is, light- and dark-adapted thresholds differed by 2 to 3 log units for measurements made in the periphery and perifovea (beyond approximately 10°), whereas light- and dark-adapted thresholds were similar at the fovea. Subjects 4, 5, and 6 had light- and dark-adapted thresholds that generally fell within the normal range at all locations. The

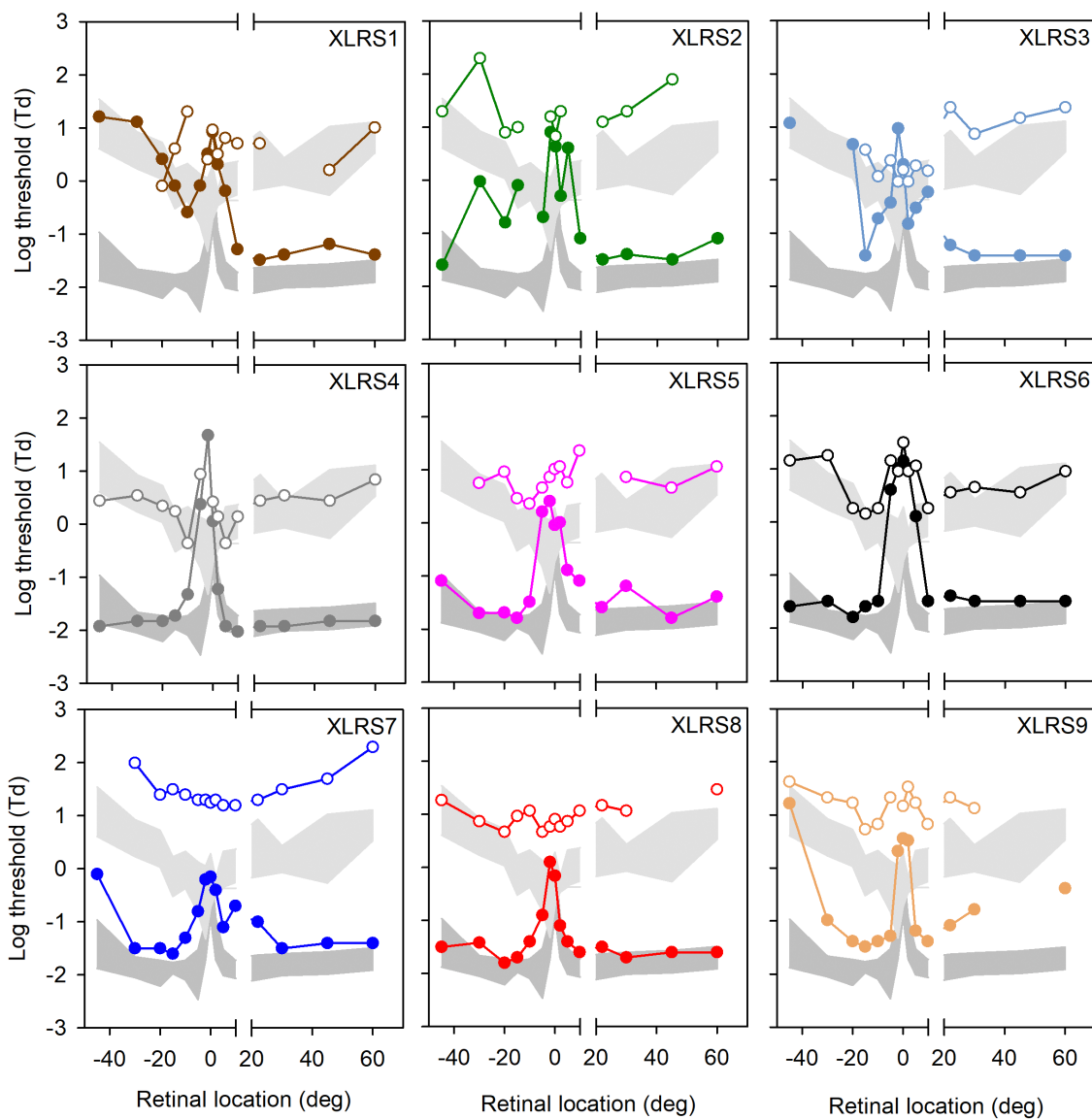


FIGURE 1. Luminance threshold (log Trolands) for each subject with XLRS is shown for measurements made under dark-adapted conditions (filled symbols) and light-adapted conditions (open symbols; 5 cd/m² background). Data under these conditions are shown as a function of retinal location (x-axis), where negative values represent data from the temporal retina and positive values represent data from the nasal retina. The break in the x-axis denotes the location of the optic nerve head. The subjects are color coded according to the designations in the Table. The gray regions mark the normal dark-adapted range (lower dark gray regions) and light-adapted range (upper light gray regions).

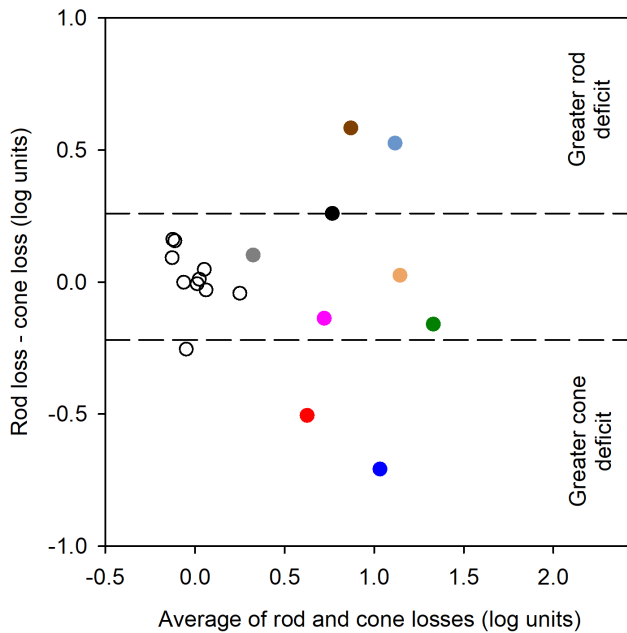


FIGURE 2. Bland-Altman³¹ plot comparing rod and cone sensitivity loss for each subject. Rod- and cone-pathway sensitivity losses were estimated as described in the text. Dashed lines mark the 95% limits of agreement for the control subjects. Data points falling above the *upper dashed line* indicate a significantly greater rod sensitivity loss, whereas data points falling below the *lower dashed line* represent a significantly greater cone sensitivity loss.

other subjects with XLRS had threshold elevations, with two subjects having somewhat greater elevations under light-adapted conditions, compared to dark-adapted conditions (subjects 7 and 8).

Figure 2 shows the relative light- and dark-adapted sensitivity loss (threshold elevation) for each subject in the form of a Bland-Altman plot.³¹ For both light- and dark-adapted measurements, sensitivity losses were quantified and compared as follows: (1) each XLRS subject's sensitivity value at each visual field location was subtracted from the normal average at the corresponding location (i.e., Δ normal); (2) each XLRS subject's sensitivity losses for all locations were averaged across the field to produce a single (mean) sensitivity loss for each subject; (3) the average light- and dark-adapted sensitivity loss for each subject with XLRS is plotted as the x-axis of Fig. 2; (4) the mean light-adapted sensitivity loss was subtracted from the mean dark-adapted sensitivity loss for each subject with XLRS and is plotted as a function of the average loss in Figure 2 (y-axis). A similar procedure was performed for the control subjects (comparing each control subject to the control average; Fig. 2 open circles) to generate the 95% limits of agreement (dashed lines) shown in Figure 2. Thus a rod – cone loss of 0 indicates equal losses within the two pathways, whereas positive and negative values represent greater rod or cone loss, respectively. Figure 2 shows that most subjects with XLRS had approximately equivalent sensitivity losses within the rod- and cone-pathways (approximately 0.90 log units for each measure). Two subjects (7, 8) had greater cone sensitivity loss compared to rod sensitivity loss. This is also apparent in their data shown in Figure 1. Two other subjects (1 and 3) had slightly greater rod sensitivity loss compared to cone sensitivity loss. The validity of this finding is somewhat

uncertain, because threshold was not measurable at several peripheral field locations for these subjects, which created a ceiling effect. Overall, psychophysical measurements of rod and cone function are similarly affected in our sample of subjects with XLRS.

Figure 3 plots log threshold as a function of the log background illuminance (adaptation level) for each subject with XLRS, compared to the normal range (gray regions). Measurements performed across the visual field were grouped into four regions to simplify visualization (i.e., periphery, perifovea, parafovea, fovea). Data for each subject were fit with Equation 1, which are represented by the solid curves. For measurements in the peripheral field (15° to 60°), seven of the nine subjects had thresholds that were nearly normal or within the normal range. For these seven subjects, thresholds were within the normal range under dark-adapted conditions (leftmost data point) and at the upper limit of normal, or slightly outside of the normal range, for the highest illuminance background (rightmost data point). The two exceptions were subjects 3 and 9, who had threshold elevations (approximately 0.5 log units) under dark-adapted and low background illuminance conditions. For measurements in the perifoveal field (5° – 10° eccentricity), all subjects had threshold elevations under dark-adapted and low background illuminance conditions, as well as for high illuminance conditions. For moderate background illuminances, subjects were either within the normal range or modestly elevated. A similar pattern was observed for measurements in the parafovea (2° eccentricity): threshold tended to be more elevated at low and high background illuminances compared to moderate background illuminances. For foveal measurements, seven of the nine subjects had thresholds that were within the normal range for dark-adapted and low retinal illuminance conditions and all subjects with XLRS had abnormally elevated thresholds for the highest retinal illuminances. For the control subjects, the slope of the ascending limb of the threshold-versus-illuminance (TvI) functions appears to increase as measurements are performed further from the fovea. In contrast, the fits for the subjects with XLRS appear similar across the visual field. This results in the XLRS functions having a normal appearance in the periphery, but being abnormally steep in the perifovea, parafovea, and fovea. These patterns can also be seen by comparing the mean data (\pm SEM) for the control subjects and subjects with XLRS, as shown in the supplementary material (Supplementary Fig. S1). The fit parameters are quantified and discussed below.

The left column of Figure 4 illustrates the effect of altering each of the model parameters on the shape and placement of the TvI curve, whereas the right column provides estimates of the model fits for the subjects. Each circle represents a different subject with XLRS and the gray regions represent the normal range. The top row shows that increasing T_0 shifts the TvI function uniformly upward on log-log coordinates (the black curve represents a hypothetical control, whereas the red curve represents a hypothetical subject with XLRS). The right panel shows that the subjects with XLRS had dark-adapted thresholds (T_0) that ranged from normal to elevated, which is also apparent in Figure 3. Averaging across all subjects with XLRS and the four visual field regions, T_0 was elevated by approximately 1 log unit. A repeated measures analysis of variance (ANOVA) was performed to compare T_0 between the XLRS group and the control group across the four visual field locations. The ANOVA indicated a significant effect of subject group

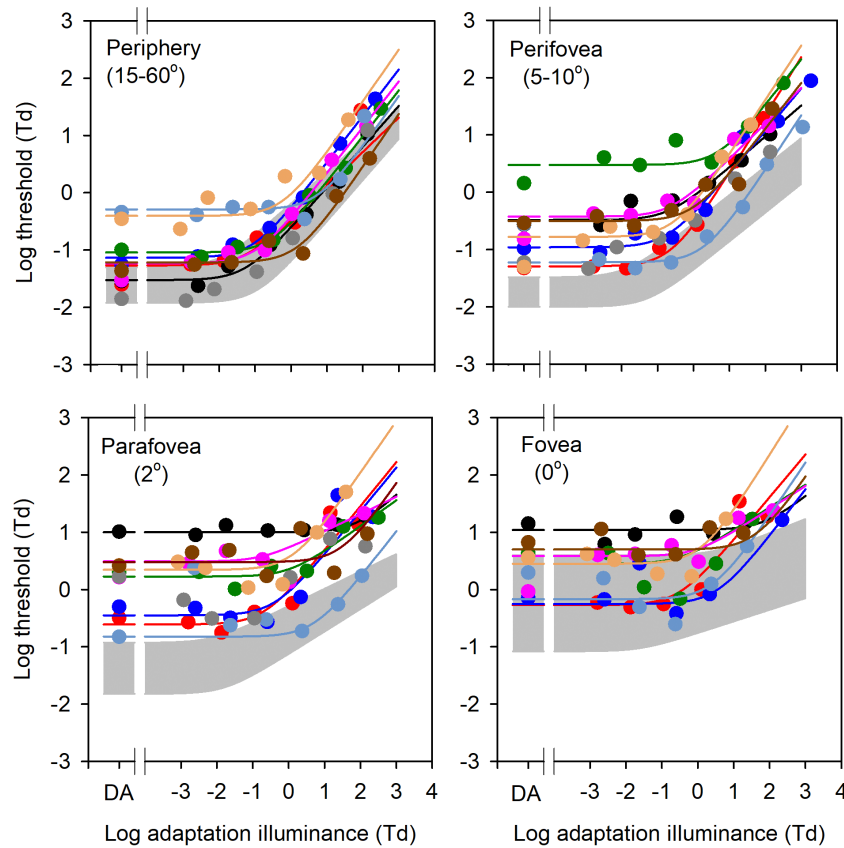


FIGURE 3. Threshold illuminance (log Trolands) is plotted as a function of the adaptation illuminance (log Trolands) for each subject with XLRS and the range of normal control data (gray regions). Data are shown for each visual field region, as indicated in the panels and defined in the text. The solid curves are fits of Equation 1 to the data.

($F = 48.40$, $P < 0.001$) and location ($F = 54.40$, $P < 0.001$); there was a significant interaction between group and location ($F = 6.26$, $P = 0.001$). Holm-Sidak pairwise comparisons indicated statistically significant differences in T_0 between the XLRS and control groups at all visual field locations (all $t > 3.13$; $P < 0.004$).

The middle row (left) shows that increasing A_0 shifts the TvI function rightward but does not elevate the dark-adapted threshold. A_0 provides an estimate of “dark light” or neural noise within the visual pathway. The right panel shows that the subjects with XLRS had A_0 values that ranged from normal to elevated, but the elevation appears somewhat greater at more central field locations (fovea, parafovea). Averaging across all subjects with XLRS and the four visual field regions, A_0 was elevated by approximately 1.6 log units. ANOVA was performed to compare A_0 between the XLRS and control groups across the four visual field locations, which indicated a significant effect of subject group ($F = 42.38$, $P < 0.001$), but not location ($F = 0.66$, $P = 0.66$); there was a significant interaction between group and location ($F = 6.51$, $p < 0.001$). Holm-Sidak pairwise comparisons indicated statistically significant differences in A_0 between the XLRS and control groups at all visual field locations (all $t > 2.66$; $P < 0.01$).

The bottom row shows that increasing n results in a steeper slope of the ascending portion of the TvI curve (left panel). The right panel shows that the subjects with XLRS had slope values (n) that ranged from normal to elevated, but the elevation appears greater at more central field loca-

tions (fovea, parafovea, perifovea). The mean value of n for the subjects with XLRS was relatively constant across the visual field: 0.73, 0.67, 0.77, 0.80 for measurements in the fovea, parafovea, perifovea, and periphery. In contrast, the value of n increased systematically from the fovea to the periphery for the controls: 0.24, 0.35, 0.55, 0.65 for measurements in the fovea, parafovea, perifovea, and periphery. ANOVA was performed to compare n between the XLRS and control groups across the four visual field locations. ANOVA showed a significant effect of subject group ($F = 35.13$, $P < 0.001$) and location ($F = 25.32$, $P < 0.001$); there was a significant interaction between group and location ($F = 9.79$, $P < 0.001$). Holm-Sidak pairwise comparisons indicated statistically significant differences in n between the XLRS and control groups at all visual field locations (all $t > 2.50$; $P < 0.02$). When fitting TvI functions, it is sometimes assumed that $n = 1$. Although this is often a valid assumption, the data of Figure 4 indicate that this is not always the case for our experimental conditions. This can also be seen in the supplementary data (Supplementary Fig. S2), which compares the fits of Equation 1 under conditions in which n is a free parameter (black) and when it is set to 1.0 (red). Allowing n to vary improved the fits for the control subjects but had little effect on the fits for the subjects with XLRS, because their data generally followed a slope of approximately 1.0 throughout the field (cf., Fig. 4, bottom).

Figure 5 compares the mean (solid line) and range (dashed lines) of retinal thickness for the subjects with XLRS and control subjects (shaded) within the central 24° along

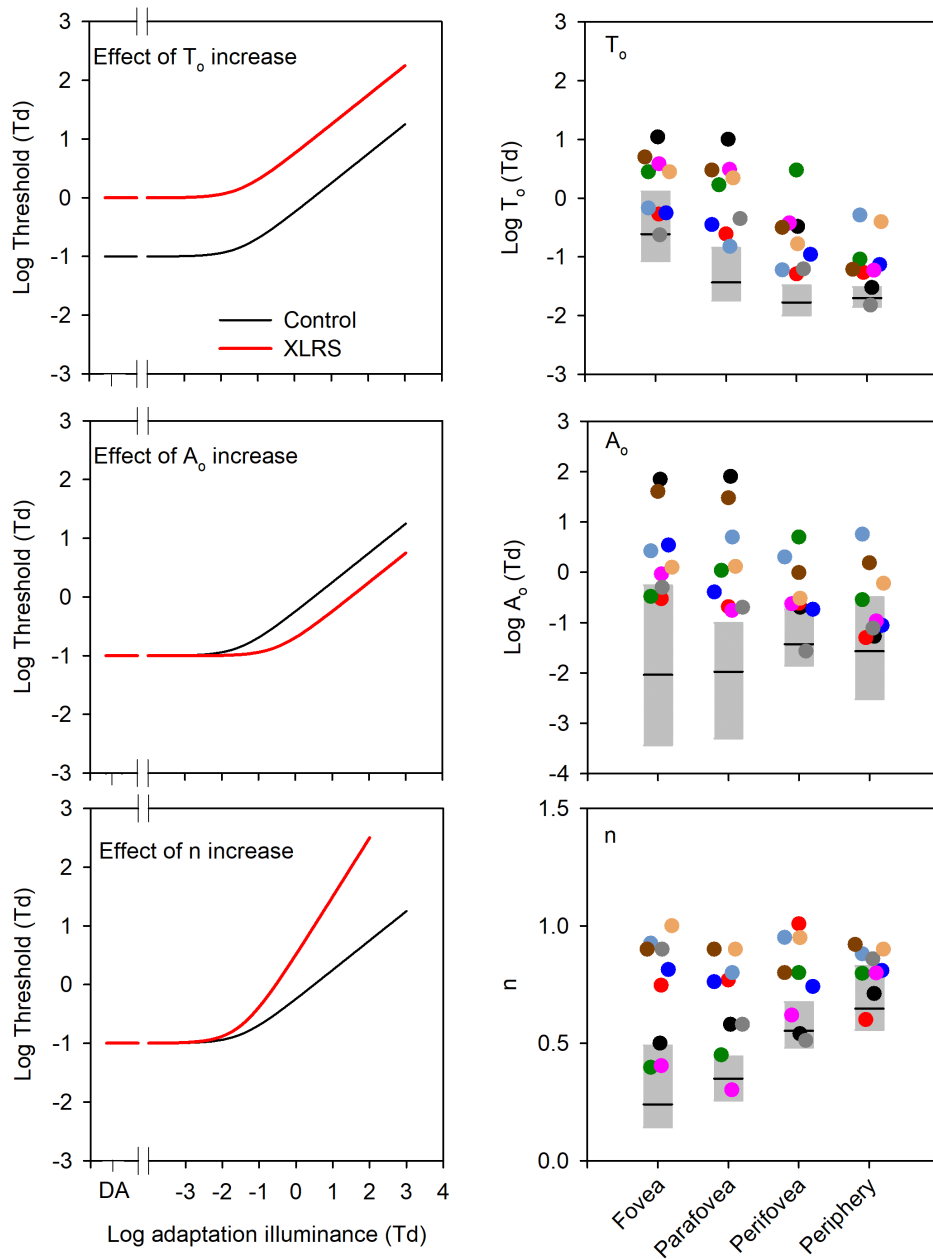


FIGURE 4. The parameters of the fits of Equation 1 are shown for each subject with XLRs (right column) and the effects of altering the parameters on the TvI curves are shown in the left column. The *black curve* represents a hypothetical control subject and is identical in each plot. The *red curves* illustrate the results of a hypothetical subject with XLRs who has a 1 log unit increase in T_0 (top) or A_0 (middle). The *lower panel* shows the effect of increasing n from 0.5 to 1. The *gray regions* in the right column represent the ranges of normal and the horizontal bars represent the control means. The *top panel* shows the values for T_0 , the *middle panel* shows the values of A_0 , and the *bottom panel* shows the values of n .

the horizontal meridian. The top panel shows considerable variation in total retinal thickness among the subjects with XLRs, with some being abnormally thick due to schitic cavities within the central macula. Other subjects with XLRs had total retinal thinning in some areas. The middle panel shows that all of the subjects with XLRs had thinning of the ONL⁺ within the central 20°. The bottom panel shows OS⁺ thinning, on average, throughout the central 24°. Overall, thinning of the ONL⁺ was most apparent in this group of subjects with XLRs.

Figure 6 shows structure-function associations under dark-adapted (left) and light-adapted (right) conditions for each subject with XLRs and for the controls (gray region). The dashed lines represent the linear model described above that predicts that normalized ONL⁺ × OS⁺ is linearly related to sensitivity loss (note the log x-axis).³⁰ The model assumes that sensitivity is limited by quantum catch, which is proportional to the product of the number of surviving photoreceptor cells and the length of their outer segments. This model has been translated vertically and horizontally to

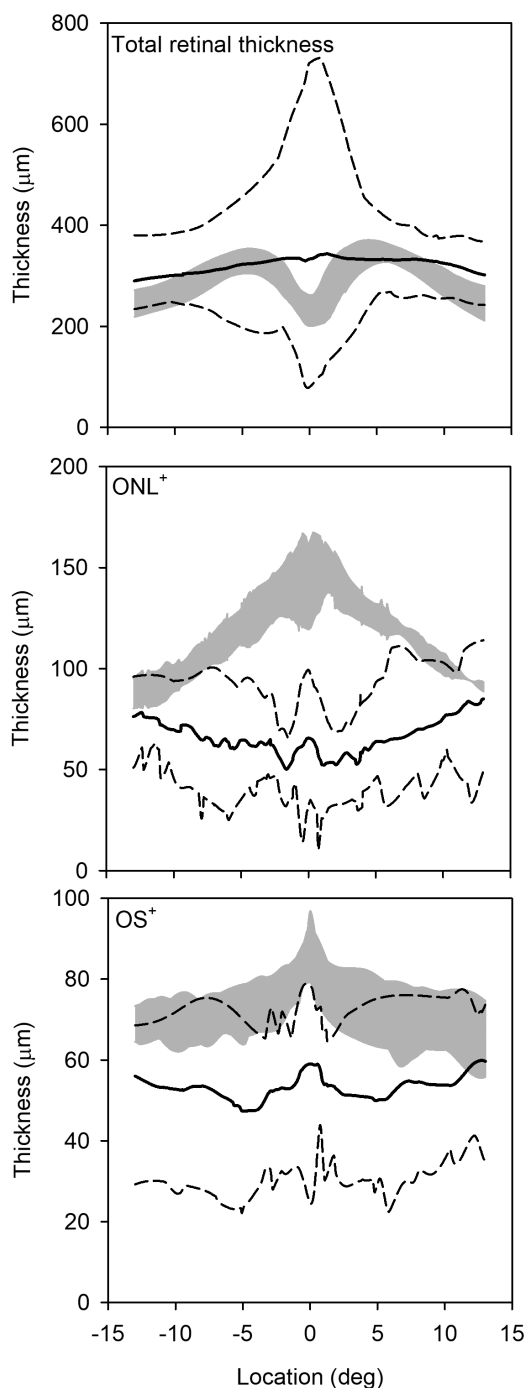


FIGURE 5. Mean (solid lines) and range (dashed lines) retinal thickness is plotted as a function of retinal location for the subjects with XLRS. The gray regions represent the range of normal. The top panel shows the total retinal thickness, the middle panel shows the ONL⁺ thickness, and the bottom panel shows the OS⁺ thickness.

capture the normal variability marked by the gray box (control range). There was a significant correlation between the normalized ONL⁺ × OS⁺ and sensitivity loss for the subjects with XLRS under both dark-adapted (Spearman's $\rho = 0.51$, $P = 0.003$) and light-adapted conditions (Spearman's $\rho = 0.57$, $P < 0.001$). With few exceptions, data for the subjects with XLRS measured at all locations fall within the model prediction under both dark- and light-adapted condi-

tions. This finding indicates that sensitivity is reduced by an amount that is related to, and predicted by, the amount of ONL⁺ × OS⁺ thinning. Subjects with considerable ONL⁺ × OS⁺ thinning (e.g., subject 6) had the greatest sensitivity loss, whereas subjects with relative ONL⁺ × OS⁺ thickness preservation had less sensitivity loss. We note that the primary location of the macular schitic cavities in this sample of subjects with XLRS was in the inner nuclear layer and that the ONL was abnormally thin (Fig. 5). Nevertheless, small areas of ONL thickening, or thinning due to Diamox treatment, could affect the structure-function relationships shown in Figure 6.

DISCUSSION

This study evaluated luminance thresholds under various levels of light adaptation, as well as the association between threshold and outer-retinal structure, in subjects with XLRS who have known *RS1* gene mutations. The primary findings of the study are that (1) subjects with XLRS generally have threshold elevations under all adaptation conditions in the macula; (2) the magnitude of the abnormality varies among subjects and depends on the adaptation level; (3) although elevated, thresholds are measurable for most field locations, even those locations falling within areas of schitic cavities; (4) thresholds are associated with outer-retinal structure under both light- and dark-adapted conditions, for all visual field locations. These findings were apparent for all subjects with XLRS, with no obvious genotype correspondence. It should be noted, however, that small sample size and genetic heterogeneity precludes genotype-phenotype correlations.

A dark-adapted ERG that is electronegative or has a reduced b/a wave ratio is a common feature of XLRS. This ERG finding is associated with retinal diseases that result in night blindness, such as the complete form of congenital stationary night blindness and melanoma associated retinopathy. Despite their reduced b/a wave ratio, subjects with XLRS generally do not complain of nyctalopia and the dark-adapted thresholds obtained in this report support relative preservation of visual function under scotopic conditions. Relative to the control mean, dark-adapted thresholds were elevated by approximately 1 log unit in our subjects with XLRS, but four subjects with XLRS (44%) had dark-adapted thresholds in the normal range. This finding is consistent with a previous report¹¹ showing that dark-adapted threshold for a full-field, short-wavelength luminance flash ranged from normal (three subjects with XLRS) to mildly elevated (up to 0.6 log units; four subjects with XLRS).

The subjects with XLRS also had threshold elevations under photopic conditions. Indeed, comparison of rod- and cone-pathway sensitivity loss indicated approximately equal abnormalities within these pathways. Two possible exceptions are subjects 7 and 8 whose cone sensitivity loss somewhat exceeded their rod sensitivity loss. Interestingly, these two subjects share the c.208G>A; p.Gly70Ser mutation. However, given the small sample size and genetic heterogeneity of our subjects, it is not possible to determine whether genotype can predict the relative loss of rod and cone sensitivity. It should also be noted that this approach of analyzing global rod and cone sensitivity cannot identify localized areas where rod and cone sensitivity may differ. The power of the present approach is that measurements were obtained from the same cohort of subjects with XLRS using a single instrument, which

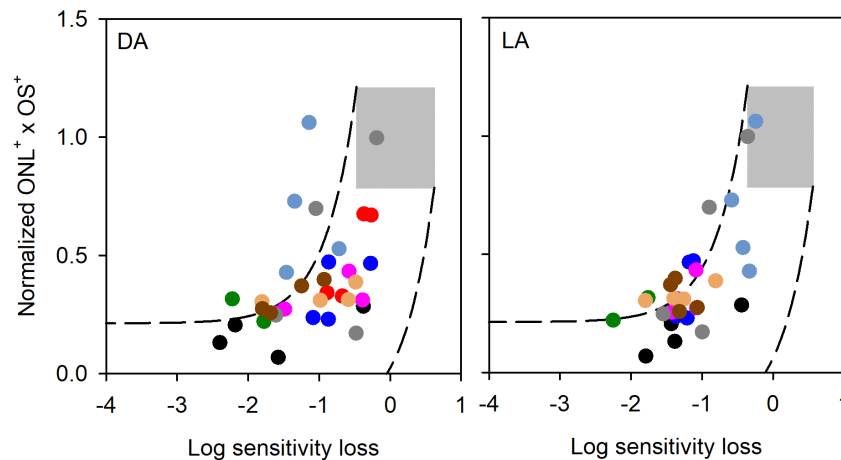


FIGURE 6. Normalized $ONL^+ \times OS^+$ thickness is plotted as a function of sensitivity loss for each subject with XLRs (measured at the four retinal areas) under dark-adapted (*left*) and light-adapted (5 cd/m^2 ; *right*) conditions. The *gray regions* represent the normal ranges and the *dashed lines* represent the prediction of the linear model as described in the text, which has been translated vertically and horizontally to capture the normal variability.

permits a more direct comparison of function within the cone- and rod-pathways. We note that cone-pathway abnormalities in XLRs are not unexpected, because the flicker ERG is typically reduced in amplitude and delayed in these individuals.²⁰

Comparison of threshold across all adaptation levels (i.e., TvI functions) indicated an unusual relationship within the macula (0 to 20°) for the subjects with XLRs. Specifically, the TvI curves were abnormally steep, having a generally constant slope (n) throughout the visual field. The average slope of the TvI curve for the subjects with XLRs within the central 20° ($n = 0.72$) was similar to that of the normal control slope ($n = 0.65$) measured in the periphery (20° – 60°). A slope of 1.0 indicates Weber adaptation, such that doubling the adaptation illuminance results in a doubling of threshold. Data from several of the subjects with XLRs approximated Weber adaptation in the fovea and parafovea, which was not observed in any of the control subjects. Instead, the control subjects had slopes that more closely approximated DeVries-Rose adaptation (slope of 0.5), which is driven by quantal fluctuation in the background.^{32,33} Thus, in the fovea and parafovea, the control data suggest that threshold may be quantal-noise-limited (DeVries-Rose adaptation), which is not the case for the subjects with XLRs (Weber-law adaptation). In addition, the steep slope of the TvI curves for the subjects with XLRs produces a complex pattern of threshold elevation. In the fovea, parafovea, and perifovea, threshold elevation was larger at low adapting illuminance (average of 0.86 log units) and at high adapting illuminance (average of 0.93 log units), compared to moderate adapting luminance (average of 0.59 log units). In contrast, threshold was similarly elevated at all adaptation levels for peripheral field measurements (average of 0.46 log units).

The loss of sensitivity under dark-adapted and light-adapted (5 cd/m^2) conditions was well predicted by the linear model proposed previously to describe structure-function relationships in patients with retinitis pigmentosa.^{28–30} Specifically, a decrease in $ONL^+ \times OS^+$ thickness was associated with a loss of photopic and scotopic sensitivity in our subjects with XLRs. This finding is consistent with a previous report⁵ that showed that microperimetric

sensitivity is highly correlated with outer segment thickness measured by OCT in subjects with XLRs. The loss of $ONL^+ \times OS^+$ thickness was a consistent finding among our subjects with XLRs (all nine subjects had areas of thinning). Retinal thinning commonly occurs in older individuals who have XLRs as the retina becomes atrophic, but retinal atrophy was not a characteristic of our sample. Indeed, $ONL^+ \times OS^+$ thinning was apparent in our younger subjects who had relatively good visual acuity (e.g. subject 1 who was 18 years old with a VA of 20/66 Snellen equivalent). The loss of $ONL^+ \times OS^+$ thickness may limit therapeutic potential, unless treatments are capable of improving outer retinal structure. Although the loss of outer-retinal structure may not be as apparent as in some other inherited retinal degenerations, consideration of outer retinal abnormalities is warranted when designing therapies for XLRs.

In summary, thresholds are elevated, but measurable, under both light- and dark-adapted conditions in XLRs. The pattern of threshold versus adaptation level is well described by a standard threshold-versus-illuminance function. However, the slope of this function was significantly steeper than normal within the macula in XLRs. Additionally, the relationship between outer-retinal structure and threshold under both light- and dark-adapted conditions was well described by a standard linear model. This modeling suggests that threshold elevation can be predicted by the extent of outer-retinal thinning, which may guide assessments of anticipated therapeutic potential in future XLRs treatment trials.

Acknowledgments

The authors thank Neal Peachey and Botir Sagdullaev for comments on the manuscript.

Supported by the National Institutes of Health R01EY029796 (JJM), P30EY001792 (UIC DOVS), K12EY021475 (RAH); The Pangere Family Foundation (GAF); unrestricted funds from Research to Prevent Blindness (UIC DOVS).

Disclosure: **J.J. McAnany**, None; **J.C. Park**, None; **G.A. Fishman**, None; **R.A. Hyde**, None

References

- Sikkink SK, Biswas S, Parry NR, Stanga PE, Trump D. X-linked retinoschisis: an update. *J Med Genet.* 2007;44:225–232.
- Sauer CG, Gehrig A, Warneke-Wittstock R, et al. Positional cloning of the gene associated with X-linked juvenile retinoschisis. *Nat Genet.* 1997;17:164–170.
- Sieving PA, MacDonald IM, Chan S. X-Linked Juvenile Retinoschisis. In: Adam MP, Ardinger HH, Pagon RA, et al. (eds). *GeneReviews*. Seattle: University of Washington; 1993.
- Wang T, Zhou A, Waters CT, O'Connor E, Read RJ, Trump D. Molecular pathology of X linked retinoschisis: mutations interfere with retinoschisin secretion and oligomerisation. *Br J Ophthalmol.* 2006;90:81–86.
- Bennett LD, Wang YZ, Klein M, Pennesi ME, Jayasundera T, Birch DG. Structure/psychophysical relationships in x-linked retinoschisis. *Invest Ophthalmol Vis Sci.* 2016;57:332–337.
- Ambrosio L, Williams JS, Gutierrez A, et al. Carbonic anhydrase inhibition in X-linked retinoschisis: An eye on the photoreceptors. *Exp Eye Res.* 2021;202:108344.
- Duncan JL, Ratnam K, Birch DG, et al. Abnormal cone structure in foveal schisis cavities in X-linked retinoschisis from mutations in exon 6 of the RS1 gene. *Invest Ophthalmol Vis Sci.* 2011;52:9614–9623.
- George ND, Yates JR, Moore AT. X linked retinoschisis. *Br J Ophthalmol.* 1995;79:697–702.
- Roesch MT, Ewing CC, Gibson AE, Weber BH. The natural history of X-linked retinoschisis. *Can J Ophthalmol.* 1998;33:149–158.
- Pennesi ME, Birch DG, Jayasundera KT, et al. Prospective evaluation of patients with X-linked retinoschisis during 18 months. *Invest Ophthalmol Vis Sci.* 2018;59:5941–5956.
- McAnany JJ, Park JC, Fishman GA, Collison FT. Full-field electroretinography, pupillometry, and luminance thresholds in X-linked retinoschisis. *Invest Ophthalmol Vis Sci.* 2020;61:53.
- Alexander KR, Barnes CS, Fishman GA. Characteristics of contrast processing deficits in X-linked retinoschisis. *Vision Res.* 2005;45:2095–2107.
- Apushkin MA, Fishman GA, Rajagopalan AS. Fundus findings and longitudinal study of visual acuity loss in patients with X-linked retinoschisis. *Retina.* 2005;25:612–618.
- Kjellstrom S, Vijayarathy C, Ponjavic V, Sieving PA, Andreasson S. Long-term 12 year follow-up of X-linked congenital retinoschisis. *Ophthalmic Genet.* 2010;31:114–125.
- Collison FT, Fishman GA. Structural and functional monitoring of extramacular cystoid spaces in a case of X-linked retinoschisis treated with acetazolamide. *Retin Cases Brief Rep.* 2018;12:318–321.
- Peachey NS, Fishman GA, Derlacki DJ, Brigell MG. Psychophysical and electroretinographic findings in X-linked juvenile retinoschisis. *Arch Ophthalmol.* 1987;105:513–516.
- Jeffrey BG, Cukras CA, Vitale S, Turriff A, Bowles K, Sieving PA. Test-Retest Intervisit Variability of Functional and Structural Parameters in X-Linked Retinoschisis. *Transl Vis Sci Technol.* 2014;3:5.
- Bagdonaite-Bejarano L, Hansen RM, Fulton AB. Microperimetry in three inherited retinal disorders. *Semin Ophthalmol.* 2019;34:334–339.
- Cukras C, Wiley HE, Jeffrey BG, et al. Retinal AAV8-RS1 gene therapy for X-linked retinoschisis: initial findings from a phase I/IIa trial by intravitreal delivery. *Mol Ther.* 2018;26:2282–2294.
- Bowles K, Cukras C, Turriff A, et al. X-linked retinoschisis: RS1 mutation severity and age affect the ERG phenotype in a cohort of 68 affected male subjects. *Invest Ophthalmol Vis Sci.* 2011;52:9250–9256.
- Simunovic MP, Hess K, Avery N, Mammo Z. Threshold versus intensity functions in two-colour automated perimetry. *Ophthalmic Physiol Opt.* 2021;41:157–164.
- Kalloniatis M, Harwerth RS. Spectral sensitivity and adaptation characteristics of cone mechanisms under white-light adaptation. *J Opt Soc Am A.* 1990;7:1912–1928.
- Hood DC, Greenstein V. Models of the normal and abnormal rod system. *Vision Res.* 1990;30:51–68.
- Park JC, Chen YF, Liu M, Liu K, McAnany JJ. Structural and Functional Abnormalities in Early-stage Diabetic Retinopathy. *Curr Eye Res.* 2020;45:975–985.
- McAnany JJ, Park JC, Liu K, et al. Contrast sensitivity is associated with outer-retina thickness in early-stage diabetic retinopathy. *Acta Ophthalmol.* 2020;98:e224–e231.
- Anastasakis A, McAnany JJ, Fishman GA, Seiple WH. Clinical value, normative retinal sensitivity values, and intrasession repeatability using a combined spectral domain optical coherence tomography/scanning laser ophthalmoscope microperimeter. *Eye (Lond).* 2011;25:245–251.
- Hood DC, Cho J, Raza AS, Dale EA, Wang M. Reliability of a computer-aided manual procedure for segmenting optical coherence tomography scans. *Optom Vis Sci.* 2011;88:113–123.
- Jacobson SG, Aleman TS, Cideciyan AV, et al. Identifying photoreceptors in blind eyes caused by RPE65 mutations: Prerequisite for human gene therapy success. *Proc Natl Acad Sci U S A.* 2005;102:6177–6182.
- Jacobson SG, Cideciyan AV, Aleman TS, et al. Usher syndromes due to MYO7A, PCDH15, USH2A or GPR98 mutations share retinal disease mechanism. *Hum Mol Genet.* 2008;17:2405–2415.
- Rangaswamy NV, Patel HM, Locke KG, Hood DC, Birch DG. A comparison of visual field sensitivity to photoreceptor thickness in retinitis pigmentosa. *Invest Ophthalmol Vis Sci.* 2010;51:4213–4219.
- Bland JM, Altman DG. Statistical methods for assessing agreement between two methods of clinical measurement. *Lancet.* 1986;1:307–310.
- Barlow HB. Increment thresholds at low intensities considered as signal/noise discriminations. *J Physiol.* 1957;136:469–488.
- Rose A. The sensitivity performance of the human eye on an absolute scale. *J Opt Soc Am.* 1948;38:196–208.